Journal of Alloys and Compounds, 191 (1993) 179–186
JALCOM 522

The effect of vacuum annealing on the hydriding kinetics of zirconium

J. Bloch[a], I. Jacob[b] and M.H. Mintz[a,b]
[a]*Nuclear Research Center – Negev, P. O. Box 9001, Beer-Sheva (Israel)*
[b]*Ben Gurion University of the Negev, Beer-Sheva (Israel)*

(Received June 22, 1992)

Abstract

The effects of vacuum preannealing on the hydriding kinetics of zirconium metal at 400 °C and 1 atm hydrogen pressure were studied using combined metallographic and kinetic measurements. Two stages were identified in the reaction kinetics: a fast initial stage in which the apparent front velocity was 70 μm min^{-1} and a second stage in which the front velocity gradually decreased until it stabilized around 8 μm min^{-1}. During the fast stage a special topochemical development of the hydride was observed, with the hydride progressing along grain boundaries which were previously oxidized during the vacuum annealing. This relatively fast process continued until a hydride overlayer was formed on the sample surface. The spatial extent of this stage was thus of the order of the grain size (around 40 μm). During the second stage of the hydriding the rate-controlling step was the diffusion of hydrogen through the product layer leading to a decrease in the apparent reaction rate. Hence, the main effect of the vacuum preannealing on the hydriding rate was introduced through grain boundary oxidation, affecting the initial rapid stage.

1. Introduction

The reaction of hydrogen gas with zirconium metal to form zirconium hydride has been extensively studied during the last three decades due to its technological importance in the nuclear industry. Hydrogen embrittlement of the Zircalloy cladding of fuel elements in water-cooled nuclear reactors has been identified as the origin of premature failures of the fuel rods in many cases [1].

The hydriding reaction kinetics have been studied by many investigators in an attempt to establish the reaction mechanism [2–6] and to determine how it is affected by the oxide layer [4, 7], catalyst addition [5] or the presence of water vapor in the hydrogen [4, 8].

The kinetics measured by various investigators have been found to follow different rate laws. Different rate-limiting steps have been determined for the reaction. Thus, for the temperature range 200–400 °C, Gulbransen and Andrew [2] measured a parabolic rate law which they associated with the diffusion of hydrogen into the metal; Belle *et al.* [3] interpreted their parabolic kinetics as the result of diffusion through a product layer. Une [4] found a linear rate law which was attributed to a phase boundary rate-limiting step. Kuus and Martens [5] observed a logarithmic rate law (diffusion in the δ-hydride phase) and Naito [6] proposed a surface-controlled reaction. (It should be noted that the later study was performed on metal surfaces which were cleaned under ultrahigh vacuum conditions and were hydrided at very low hydrogen pressures.)

It is interesting, however, that despite the different rate laws associated with different rate-limiting steps, the activation energy measured was practically the same (between 16.3 [4] and 17.2 kcal mol^{-1} [3]).

Little is known about the relationship between the zirconium metal microstructure and its hydriding kinetics. It has been shown for many metal–hydrogen systems that microstructural changes, induced for example by heat treatments, may significantly affect the hydriding kinetics and mechanism. Thus, for uranium [9], vacuum annealing above 600 °C resulted in both grain growth and acceleration of the hydride–metal reaction front velocity. For zirconium, vacuum annealing is associated with gettering properties in addition to grain growth. Due to the high reactivity of the metal, oxygen is accumulated in the zirconium during heat treatments even under high vacuum conditions (*i.e.* at pressures as low as 10^{-7} torr [10]). Two types of oxide phase development in zirconium have been found under low pressure conditions [11]. The first (designated type I) is the random formation of intragranular oxide nuclei. The surface density of these nuclei depends on the orientation of the grain. The second mode of oxide

0925-8388/93/$6.00

growth, designated as type II, is more important in the present case. It involves the formation of needle-like oxide nuclei originating at a grain boundary oxide layer. These needle-like nuclei grow perpendicularly to the grain boundaries until they overlap, consuming the entire grain.

It was found that pre-dissolved oxygen, accumulated in the zirconium during vacuum annealing as described above, may considerably modify the rate of subsequent oxidation. In general, the kinetics of the reaction of oxygen with free metal are found to be slower than with samples containing pre-dissolved oxygen [12, 13]. Osthagen and Kofstad [14] found, for 800 °C oxidation, that the rate of oxidation increased with pre-dissolved oxygen content up to a level of about 12–15 at.%. Beyond this range, no effect was found.

No data are available on the effect of pre-dissolved oxygen on the kinetics and mechanism of the hydriding reaction of zirconium.

In the present work, the hydriding kinetics of vacuum-annealed bulk Zr metal were studied at 400 °C and at 1 atm hydrogen pressure. Different sample geometries were used. The kinetics measurements were combined with metallographic examinations of partially hydrided samples in an attempt to relate the metal microstructure and oxide distribution to the hydriding kinetics. These combined measurements have been shown previously to yield internal kinetic parameters [15] in the hydriding reactions of various metals such as uranium [16], titanium [17] and hafnium [18] as well as in intermetallics [19].

2. Experimental details

2.1. The apparatus

Experiments were performed in a quartz P–V–T system pumped with a diffusion pump down to a base pressure of 1×10^{-7} Torr. Kinetics were measured by following the hydrogen pressure changes using a capacitance pressure transducer equipped with an external offset voltage supply to increase measurement sensitivity. Measurements were made under constant volume conditions. However, the chamber volume and sample weight were adjusted in such a way that the pressure change due to an overall reaction will not exceed 10% of the applied pressure. Thus the reaction kinetics were measured under almost invariable pressure conditions. The transducer output was connected to a data acquisition system operated by a personal computer. The chamber temperature was maintained constant by an external furnace controlled by a Eurotherm controller. The temperature was measured by a chromel–alumel thermocouple.

2.2. Sample preparation

Samples of defined geometry and dimensions were cut from 99.8% Zr ingot. Chemical analysis of the material showed that the main impurities were Fe (800 ppm), Hf (400 ppm), Co (less than 200 ppm) and Cr (100 ppm). Other metals (Cu, V, Ba, Cd, Mo, Ni, Ti, Zn, Ca, Mg, Sr and Mn) were found to be under 70 ppm concentrations.

Preliminary experiments were performed in order to determine the conditions under which preheating should be performed. In general, preheating of the metal prior to the hydriding measurements is needed to remove adsorbed gases (outgassing) and to activate the outermost native oxide layer, leading to reduced incubation periods and more reproducible kinetics [9]. In these preliminary experiments it was found that increasing preheating temperatures affected both the incubation periods and the absorption kinetics. The effect of the duration of preheating at a certain fixed temperature was also investigated. In this case the incubation periods were shortened with increased preheating times, whereas the absorption kinetics were less sensitive to this variable.

Since the reaction mechanism in this system is rather complex and sensitive to the conditions of the preheating process (as will be shown later), it was essential to apply certain constant preheating conditions throughout the study. A basic understanding of the reaction mechanism under these fixed preheating conditions may then lead to more general conclusions on the qualitative trends of the effects of variable preheating temperatures and duration on the subsequent hydriding kinetics. Hence, the choice of preheating treatment was fixed at 900 °C for 2 h. The hydriding reactions were performed at 400 °C under a hydrogen pressure of 1 atm.

In Fig. 1 the metallographic microstructure of an unreacted sample is compared with that of a sample preheated in vacuum for 2 h at 900 °C. Two significant effects are revealed by the comparison of the two samples: firstly, the average grain size is increased from about 15 to 50 μm, and secondly, oxidation of the interior of the sample is observed. Most of the oxide is developed along grain boundaries. Smaller amounts of needle-like oxide, originating at the grain boundaries, are also formed. The formation of this type of oxide (type II) under our working conditions of pressure and temperature is in accordance with the results of Paidassi and Nierlich [20] for the oxidation of zirconium under low pressures and high temperatures.

3. Results and discussion

3.1. The effect of sample geometry

The hydriding reaction of many metals in their bulk form is characterized by the development of a product

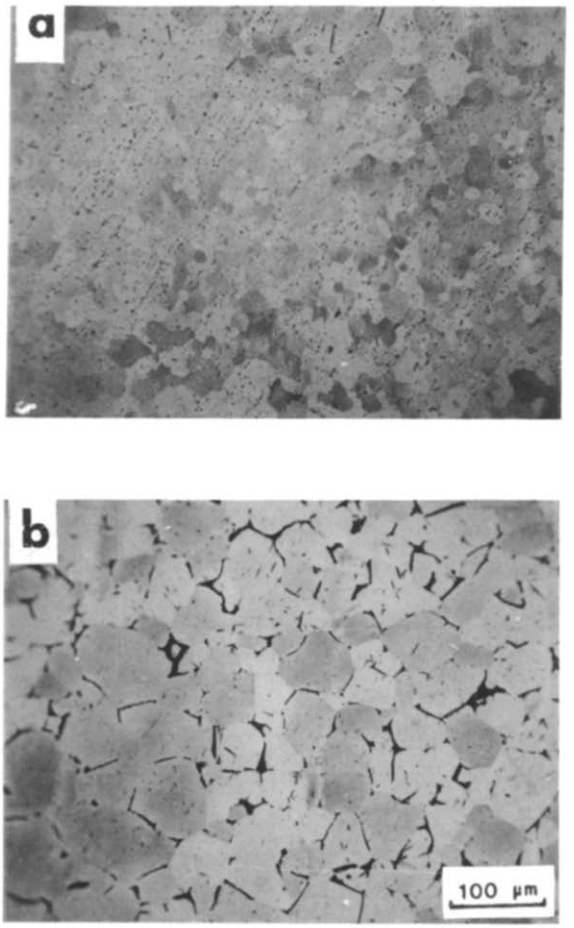

Fig. 1. Microstructure of untreated zirconium sample (a) and sample heated under high vacuum at 900 °C for 2 h (b) (the scale at the bottom applies to both micrographs).

(*i.e.* hydride) layer on the metal surface which proceeds into the bulk sample during the hydriding process. The kinetic behaviour produced by this type of reaction is known as "contracting envelope" behaviour [15]. For a parallelepiped sample of dimensions $a \times b \times c$ the time dependence of the reacted fraction α is given by a cubic polynomial equation

$$\alpha = \sum_{i=1}^{3} a_i X(t)^i \tag{1}$$

The geometric coefficients a_i are given by

$$a_1 = 2(1/a + 1/b + 1/c) \tag{2}$$

$$a_2 = -4(1/ab + 1/ac + 1/bc) \tag{3}$$

$$a_3 = 8/abc \tag{4}$$

$X(t)$ is the displacement of the product layer advanced into the sample. In general, $X(t)$ is obtained from

$$X(t) = \int_0^t U(t)\, \mathrm{d}t \tag{5}$$

Though eqn. (5) is valid over all the integration range (during the incubation period $U(t)$ is zero), it is not applicable before a continuous hydride product layer is established on the sample surface. This point is achieved at time t_1. The amount of hydride formed up to this stage is equivalent to a displacement X_0. These parameters can be combined into eqn. (5) in an attempt to define the range of application. Using these parameters eqn. (5) yields

$$X(t) = \int_{t_1}^{t} U(t)\, \mathrm{d}t + X_0 \tag{5a}$$

$U(t)$ is the product front velocity. This velocity may be time dependent (as for example in a diffusion-controlled process through a thickening product layer) or constant with time. In the latter case, eqn. (5) is simplified to

$$X(t) = U(t - t_0) \tag{6}$$

where t_0 is the time in which the reaction front would start its advance assuming it was formed instantaneously and uniformly over all the metal surface. As mentioned above, eqn. (6) is valid for $t > t_0$ and applicable for $t > t_1$.

For a contracting envelope case in planar samples in which one dimension is much smaller than the other two (*i.e.* $a \ll b, c$), eqn. (1) can be further simplified

$$\alpha = (2/a)X(t) \tag{7}$$

Hence, it is convenient to utilize thin planar samples to evaluate the time behaviour of the reaction displacement in the contracting envelope morphology. For a constant front velocity case (*i.e.* eqn. (6)), eqn. (7) yields a linear dependence of α *vs.* t, with a slope $2U/a$, *i.e.* inversely proportional to the initial thickness of the planar sample (as long as the planar approximation is valid).

In Fig. 2 a cross-section is shown near the edge of a partially hydrided sample ($\alpha = 0.25$). To confirm the occurrence of a contracting envelope morphology for the case shown in Fig. 2, the hydriding kinetics of planar samples with variable initial thicknesses were measured. Figure 3 demonstrates the kinetics of two samples of different thicknesses, namely 100 μm (Fig. 3(a)) and 530 μm (Fig. 3(b)), hydrided under the experimental conditions specified in Section 2.2. In the thinner sample the kinetics follow a linear law for the most part. This is not the case for the second, thicker sample. It is evident that here the velocity of the hydride front is faster at the beginning, decreasing as the reaction proceeds. In general, samples thinner than about 180 μm follow linear relatively fast kinetics characterized by a single constant front velocity. Increasing the sample's thickness above this value yields a non-linear kinetic behaviour with a decreasing rate. For samples

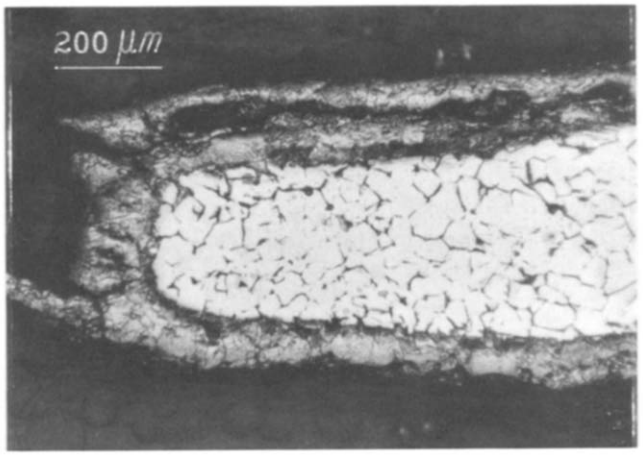

Fig. 2. Cross-section metallography near the edge of a partially hydrided ($\alpha = 0.25$) zirconium foil. The sample was preannealed under high vacuum at 900 °C for 2 h. Hydriding was performed at 400 °C under 1 atm H_2.

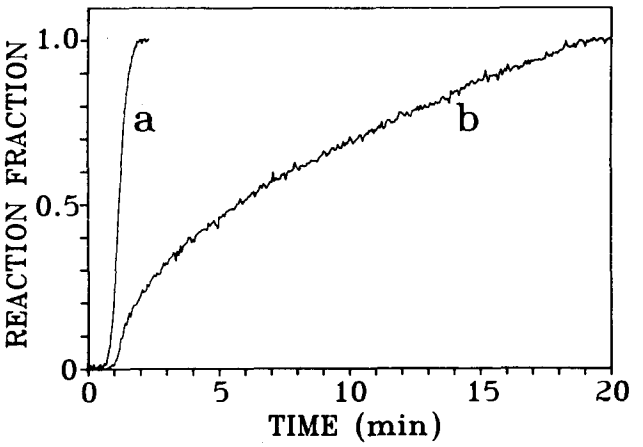

Fig. 3. Effect of sample geometry on the hydriding of Zr metal (under the same conditions of preannealing, pressure and temperature as in Fig. 2). Sample dimensions are: (a) 0.1 mm×2.1 mm×5.8 mm; (b) 0.53 mm×2.1 mm×5.8 mm.

thicker than about 500 μm two stages can be observed in the kinetic curves, as shown in Fig. 3(b). Thus it is concluded that there are two types of kinetics involved in the hydriding process which depend on sample geometry: an initial fast stage, characterizing the kinetics of a certain near-surface region (within the first 180 μm), followed by a second, slower stage, characterizing the hydriding of the bulk metal. To check this point the hydriding rate of a sample with the shape of a parallelepiped was measured. The parallelepiped's dimensions were 1.65 mm×1.79 mm×1.90 mm. Figure 4(a) demonstrates the measured kinetics of this sample. To analyse the results we used eqn. (1). Since α, a, b and c are known, each experimental point in the cubic equation can be solved to yield $X(t)$. The plot of the calculated $X(t)$ values *vs.* time is shown in Fig. 4(b). This plot displays two linear portions: an initial fast

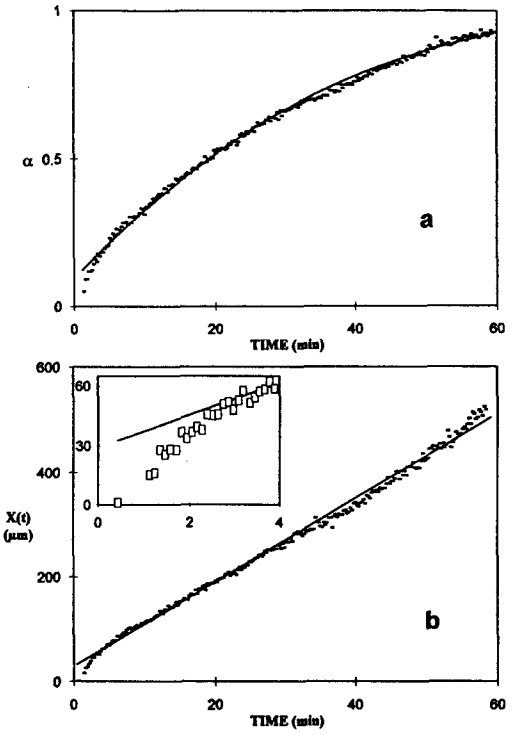

Fig. 4. (a) Hydriding kinetics of a Zr sample shaped as a parallelepiped (dimensions, 1.65 mm×1.79 mm×1.90 mm) under the same conditions as in Fig. 2. (b) Reaction front advance *vs.* reaction time: −, calculated from the experimental data using eqns. (1)–(4), ——, calculated by best-fit linear regression.

stage (for $X < 50$ μm), as demonstrated by the inset in Fig. 4(b), followed by a slower stage (for $50 < X < 450$ μm). The corresponding reaction front velocities, obtained from the slopes of the curve, are 60 and 8.0 μm min^{-1} for the initial and subsequent stages respectively (the value for the initial stage is, of course, roughly approximated).

In the intermediate range between the two linear stages (*i.e.* the fast and the slow stages) decelerating rate kinetics are observed. The relative proportions of the different stages in a certain α *vs.* t (or X *vs.* t) curve are evidently related to the dimensions of the sample. For thin (less than 100 μm) samples, the most dominant contribution displayed in the kinetic curves is the initial fast stage (*e.g.* Fig. 3(a)), whereas for thick samples, the subsequent main stage is dominating (*e.g.* Fig. 4). In order to demonstrate further the above kinetic behaviour in a case presenting both stages in comparable proportions, a sample with an intermediate thickness (530 μm) was used. Figure 5 presents the apparent reaction front velocity, obtained by taking the numerical derivative $d\alpha/dt$ as a function of reaction front displacement. Prior to differentiation, the experimental data were smoothed using cubic polynomial functions (known as cubic splines) to eliminate the effect of the experimental noise. Initially, the front velocity is relatively high (around 70 μm min^{-1}). How-

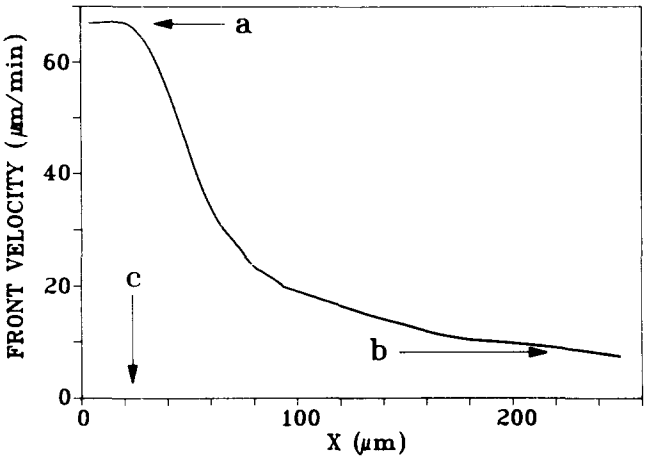

Fig. 5. Hydride front velocity, obtained by numerical time differentiation of α, *vs.* hydride penetration depth X for a foil, 530 μm thick (reaction conditions as in Fig. 2). The arrow (a) indicates the initial front velocity obtained in Fig. 6 (67 μm min^{-1}). The final asymptotic velocity shown by (b) is the velocity obtained for the relatively thick sample shown in Fig. 4 (8 μm min^{-1}). The arrow (c) shows the average grain radius (25 μm).

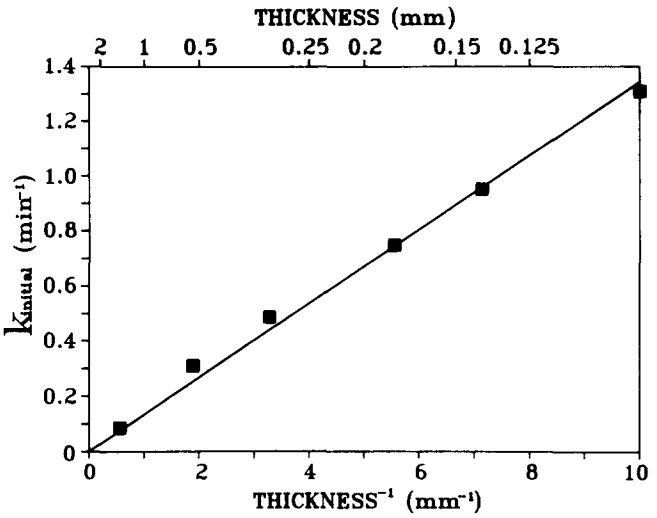

Fig. 6. Linear rate constant ($d\alpha/dt$) of the initial reaction stage for different samples as a function of the reciprocal of the sample's smallest dimension. Reaction temperature, 400 °C. Hydrogen pressure, 1 atm. All samples were preannealed under high vacuum at 900 °C for 2 h.

ever, after about 30 μm of hydride penetration the velocity drops sharply, following approximately an exponential law. A deceleration stage prevails up to 240 μm penetration where the velocity approaches an asymptotic value of 8 μm min^{-1}, in good agreement with that obtained for the cubic sample (Fig. 4).

A more accurate determination of the initial stage velocity U_i can be obtained by measuring the initial slopes of the α *vs.* t kinetic curves for different planar samples of various initial thicknesses. A plot of these slopes *vs.* reciprocal thickness yields a line with the slope $2U_i$. Figure 6 presents such a curve from which the value of $U_i = 67$ μm min^{-1} is obtained.

It is interesting to compare our results with those of Une [4] who measured the hydriding kinetics of Zircalloy-2 tubes as a function of temperature and pressure. No vacuum annealing pretreatment was reported for his work. The front velocity calculated from the experimental data obtained for the reaction is 7.5 μm min^{-1} at 400 °C for tubes of 860 μm wall thickness (the front velocity was found to be pressure independent in the range 0.2–1 atm). Considering the differences in sample composition (we used pure Zr compared with Zircalloy-2 in ref. 4) and the different experimental systems (*PVT* in our work compared with thermogravimetric measurements), this value is in very good agreement with the low main stage velocity obtained in our case for thick samples. No initial fast stage was observed in the kinetic curves shown in ref. 4 in contrast with our results. Thus it is concluded that the fast initial stage is related to the vacuum preannealing treatment.

3.2. Metallography of partially hydrided samples

In order to account for the initial fast stage observed in the front velocity, a series of metallographic examinations of partially hydrided samples was performed. One of these samples is shown in Fig. 2. Beyond the envelope of the hydride product layer, some preferred penetration of hydride extensions along the metal grain boundaries may be observed. The sample in Fig. 2 was hydrided to $\alpha = 0.25$. Decreasing the extent of partial hydriding to $\alpha = 0.1$ resulted in a thinner hydride layer. The thickness of certain areas on this layer was of the order of the metal grain size. This latter sample was mounted in a slightly tilted position (beveled) and was polished carefully to expose gradually layer by layer from the surface into the bulk. In Fig. 7, micrographs representing the hydride phase development at different depths are shown. Figure 7(a) shows a reference (unhydrided) sample. Figure 7(b) illustrates the topochemistry of a hydride which has advanced a few metal grains into the bulk. This figure may represent the incipient development of the hydride during the initial stage of the hydriding reaction. In Fig. 7(c), on the other hand, a more developed hydride phase is illustrated. The layer shown in this figure is located above the region shown in Fig. 7(b). The depth of this layer below the surface is of the order of 1–2 metal grain diameters. In the outermost surface of this sample the metal grains are fully transformed into the hydride phase (not shown in the figure).

3.3. Topochemistry and the rate-limiting step

On the basis of the above results the topochemical aspects of the hydride phase progress into zirconium

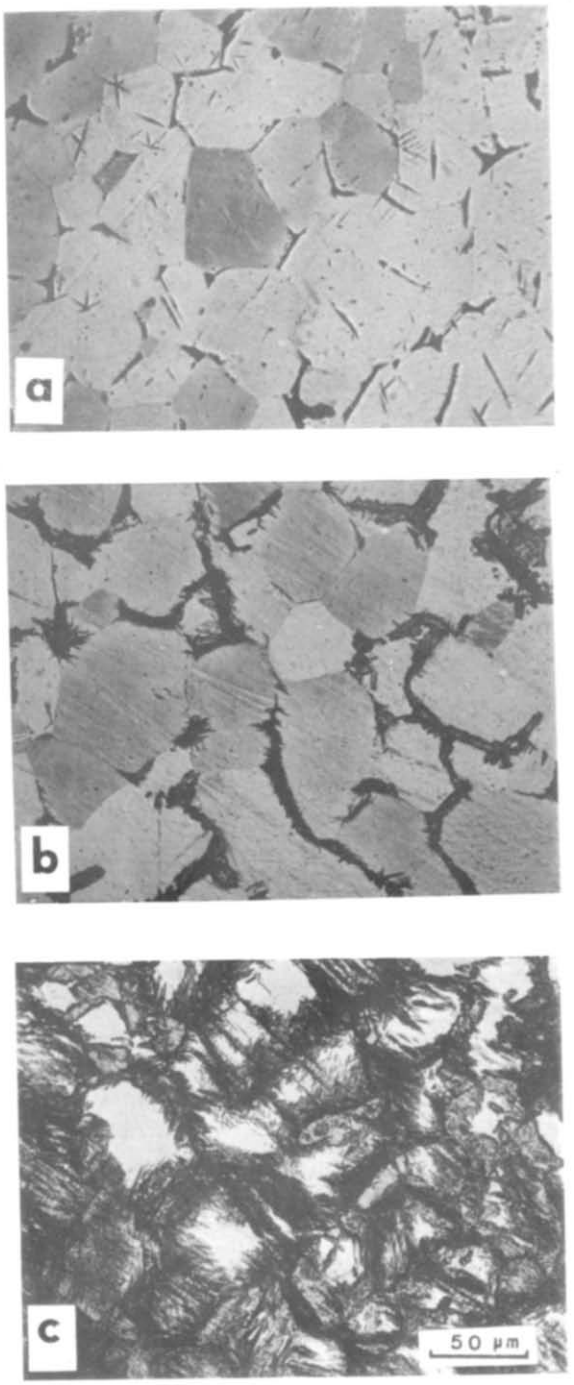

Fig. 7. Grain boundary hydriding in Zr at 400 °C and 1 atm H_2: (a) sample after vacuum annealing (10^{-6} Torr, 900 °C, 2 h); (b) hydride microstructure approximately two grain sizes below the surface (see text); (c) microstructure approximately one grain size below the surface (the scale at the bottom applies to all three micrographs).

can be deduced. Hydrogen diffuses relatively rapidly along the grain boundaries which were previously oxidized during the vacuum annealing process. A concentration gradient is built along the grain boundaries decreasing towards the sample interior. The hydride phase is formed on the circumferences of the grains and starts to advance intragranularly. The initiation of hydride nucleation occurs firstly at the near-surface region, since the hydrogen concentration build up is higher there. The initial fast kinetics displayed for vacuum-annealed zirconium may thus be accounted for by the high effective hydride front interface area in addition to the geometrical surface area of the sample. A similar kinetic behaviour was found for the hydriding of titanium under similar conditions [17]. In this case the initial fast stage was attributed to the situation in which the hydride layer has not yet developed to the full surface coverage which serves as a protective diffusion barrier [15]. It should be noted that, in the present case, there is no way to distinguish between the two topochemical paths mentioned above (*i.e.* the preferred penetration through grain boundaries resulting in intergranular advance and the creation of a uniform hydride layer moving at a fast constant velocity) from the kinetic results alone since both forms yield the same time dependence (*e.g.* linear for planar samples). However, the comparison between the initial and slower subsequent kinetics, combined with metallographic examinations of partially hydrided samples, can prove the dominant topochemistry.

The exact mechanism by which the intergranular oxide enhances the hydrogen diffusion is not clear at this stage. The oxygen may affect the diffusion coefficient of hydrogen through the metal, change the solubility limit of the hydrogen in Zr or induce microcracks used as channels for hydrogen penetration. With regard to the first possibility it is known that when the surface native oxide exceeds a certain thickness it becomes a barrier for hydrogen penetration. This is shown by the longer induction periods obtained with increasing oxide film thickness [4]. On the other hand, it has been shown that under certain conditions the oxide layer can be permeable to hydrogen [7, 8]. The complex effect of oxygen on the interaction of hydrogen with Zr is also demonstrated in the case of hydrogen solubility in Zr. Recently, the effect of oxygen on this solubility has been studied [21, 22]. It was found that the solubility at constant pressure first increases with the oxygen content then passes through a maximum. In view of the complexity of oxygen effects on the relevant parameters, the difficulties in anticipating the effect of the intergranular oxide on the hydriding kinetics are not surprising.

From Fig. 7(b) and 7(c) it is clear that a concentration gradient of intergranular hydrogen exists from the surface into the bulk. This gradient may be the result of hydrogen diffusion along grain boundaries into the metal. It should be noted, however, that the formation of the grain boundary oxide during the vacuum annealing stage is also probably a diffusion-controlled process.

Thus it is possible that the distribution of hydrogen along grain boundaries is also affected by the previously established gradient of intergranular oxide. To separate between these two possibilities, further research must be performed (*e.g.* studying the effect of preannealing time and temperature on the extent of the initial fast step in the hydriding reaction).

The rate of reaction is substantially decreased immediately after a full surface coverage layer has been formed, *i.e.* when the outermost metal grains have been fully hydrided. In Fig. 5 the arrow denoted by (c) clearly indicates that the apparent front velocity starts to fall when the penetration depth is of the order of an average grain size (25–30 μm). Hence, the product hydride forms a protective barrier to hydrogen penetration into the sample. If the hydrogen transfer rate through the hydride layer is equal to or higher than the rate of transfer through the grain boundaries, no change in the overall reaction rate is expected.

This fact points to the possibility that the rate-determining step in the main stage hydriding of zirconium (under the given conditions) is controlled by diffusion through the product hydride layer. The constant velocity (of 6.7 μm min^{-1}) attained in the second main stage can thus be associated with diffusion through a layer with an apparently constant thickness [15, 17]. It should be noted that the apparent activation energy of 16.3 kcal mol^{-1} (0.71 eV), found for the front velocity under similar conditions, corresponds well to the activation energy of hydrogen diffusion in the ϵ-hydride and in the $\delta+\epsilon$ two-phase region. This can be seen in Table 1, which summarizes the diffusion coefficients for hydrogen in zirconium hydrides (found in the literature). Except for the unusually high value found by Albrecht and Goode [24] all values fall in the range 16 ± 4 kcal (mol H)$^{-1}$.

In order to understand the possible mechanism responsible for the diffusion-controlled constant front velocity, we consider the hydrogen path from the gas phase into the hydriding area at the metal–hydride interface in relation to the hydride phase development during the hydriding process. This is shown schematically in Fig. 8. In front of the hydride–metal phase boundary

TABLE 1. Activation energies for hydrogen diffusion in zirconium hydrides

Hydride phase and composition	Activation energy (kcal mol^{-1})	Reference
δ-$ZrH_{1.54}$	12.5	23
(δ, $\delta+\epsilon$)-$ZrH_{1.6}$–$ZrH_{1.86}$	34.9	24
($\delta+\epsilon$)-$ZrH_{1.75}$	12.7	25
ϵ-$ZrH_{1.92}$	20	26
ϵ-$ZrH_{1.96}$	19.1	27
ϵ-$ZrH_{1.99}$	15	23

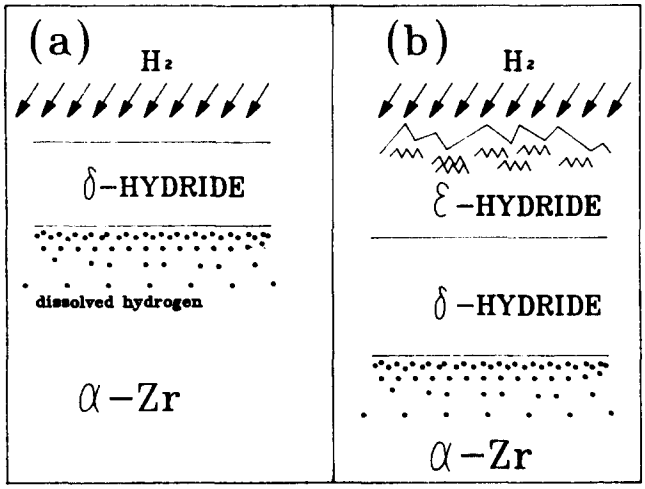

Fig. 8. Schematic representation of hydride development on Zr at 400 °C under 1 atm H_2: (a) initial stage; (b) main steady state stage.

there is always a region in which the hydrogen concentration gradient is maintained. At steady state, this region is of approximately constant width [28]. Under the given conditions of pressure and temperature the first hydride phase to be formed is the δ phase (Fig. 8(a)). The thickness of this δ phase layer is increased, together with the hydrogen concentration at the hydride–gas interface, until the ϵ phase is formed. From this point on the thickness of the δ phase will stay constant and the ϵ phase thickness will increase steadily almost until reaction completion. When the ϵ phase exceeds a certain thickness, cracks will be formed near the layer surface. Again, these cracks may follow the adherent layer in an approximately constant interval (Fig. 8(b)). Examination of fully hydrided samples reveals cracks on the surface with an approximately constant interval of 200 μm. In Fig. 2 cracks can be observed as the hydride layer exceeds approximately 50 μm.

It is either the δ phase or the ϵ phase which may have a constant thickness during the steady state stage of the kinetic process and serves as the diffusion barrier to hydrogen. There are not sufficient data to decide which of them is the actual rate-controlling layer. Further experiments under conditions in which the β phase is present are being conducted to shed more light on this question.

4. Conclusions

(1) Zr metal, annealed at 900 °C under high vacuum (10^{-6} Torr), was preferentially oxidized along grain boundaries.

(2) Subsequent hydriding at 400 °C and 1 atm H_2 displayed two-stage kinetics: an initial rapid stage followed by a slower main stage.

(3) Both the initial and main stages follow contracting envelope kinetics with apparent front velocities of about 70 and 8 μm min^{-1} respectively.

(4) During the initial rapid stage, the hydride is preferentially formed along the (oxidized) exterior grain boundaries of the metal, progressing for each grain from its boundary inward.

(5) When an external hydride layer with a thickness of about an average metal grain size is formed, the rate of reaction is drastically decreased (by almost an order of magnitude).

(6) The rate-determining step from this point on is the diffusion of hydrogen through the product hydride layer, maintaining an apparently constant thickness. This layer is composed of either the δ or ϵ hydride phases.

Acknowledgments

The technical assistance of Mr. A. Kremner is gratefully acknowledged. This work was partially supported by a joint grant from the Israel Council for Higher Education and the Israel Atomic Energy Commission.

References

1 J. A. L. Robertson, *J. Nucl. Mater., 100* (1981) 108.
2 E. A. Gulbransen and K. F. Andrew, *Metall. Trans., 185* (1949) 515.
3 J. Belle, B. B. Cleland and M. W. Mallett, *J. Electrochem. Soc., 101* (1954) 211.
4 K. Une, *J. Less-Common Met., 57* (1978) 93.
5 G. Kuus and W. Martens, *J. Less-Common Met., 75* (1980) 111.
6 S. Naito, *J. Chem. Phys., 79* (1983) 3113.
7 E. A. Gulbransen and K. F. Andrew, *J. Electrochem. Soc., 104* (1957) 709.
8 D. W. Shannon, *Corrosion (Houston), 19* (1963) 414.
9 J. Bloch and M. H. Mintz, *J. Less-Common Met., 166* (1990) 241.
10 L. Renucci and J. P. Langeron, *J. Nucl. Mater., 23* (1967) 79.
11 M. Perdereau and J. Bardolle, *C.R. Acad. Sci., Paris, 257* (1963) 2477.
12 K. H. Akram and W. W. Smeltzer, *Can. Metall. Q., 1* (1962) 41.
13 J. P. Pemsler, *J. Electrochem. Soc., 113* (1966) 1242.
14 K. Osthagen and P. Kofstad, *J. Electrochem. Soc., 109* (1962) 204.
15 M. H. Mintz and J. Bloch, *Prog. Solid State Chem., 16* (1985) 163.
16 J. Bloch and M. H. Mintz, *J. Less-Common Met., 81* (1981) 301.
17 A. Efron, Y. Lifshitz, I. Lewkowicz and M. H. Mintz, *J. Less-Common Met., 153* (1989) 23.
18 Y. Levitin, J. Bloch and M. H. Mintz, *J. Less-Common Met., 175* (1991) 219.
19 N. Bronfman, J. Bloch, M. H. Mintz, D. Sarussi and I. Jacob, *J. Alloys Comp., 177* (1991) 183.
20 J. Paidassi and J. Nierlich, *C.R. Acad. Sci., Paris, 267* (1968) 1085.
21 S. Yamanaka, T. Tanaka and M. Miyake, *J. Nucl. Mater., 167* (1989) 231.
22 M. Moalem and D. R. Olander, *J. Nucl. Mater., 178* (1991) 61.
23 J. F. Hon, *J. Chem. Phys., 36* (1962) 759.
24 W. M. Albrecht and W. D. Goode, Jr., *USAEC Report BMI-1426,* Battelle Memorial Institute, March 3, 1960.
25 K. R. Doolan, P. P. Narang and J. M. Pope, *J. Phys. F, 10* (1980) 2073.
26 R. Chang, *USAEC Report NAA-SR-5537,* Atomics International, September 15, 1960.
27 J. M. Pope, P. P. Narang and K. R. Doolan, *Phys. Chem. Solids, 42* (1981) 519.
28 J. Bloch, Z. Hadari and M. H. Mintz, *J. Less-Common Met., 102* (1984) 311.